Available online at www.sciencedirect.com
ScienceDirect
Journal of the European Ceramic Society 31 (2011) 241–248
www.elsevier.com/locate/jeurceramsoc

CO_2 gas-activated sintering of carbonated hydroxyapatites

Z. Zyman *, M. Tkachenko

Physics of Solids Department, V.N. Karazin Kharkiv National University, 4 Svobody Sq., Kharkiv 61077, Ukraine

Received 4 November 2009; received in revised form 26 August 2010; accepted 6 September 2010
Available online 20 October 2010

Abstract

Sintering compacts of carbonated hydroxyapatite (CHA) nanoparticles (3.4 wt% CO_3^{2-}) in a CO_2 flow (4 mL/min) proceeded at a temperature which was more than 200 °C lower than that for hydroxyapatite in air (1150 °C). During heating from RT to 1200 °C (5 K/min) the rate of shrinkage of the CHA compacts showed a maximum thrice as high as that in air at about 929 °C. The shrinkage correlates with a mass loss caused by the release of CO_2 due to the thermal decomposition of CO_3^{2-} ions that substitute PO_4^{3-} ions in the CHA lattice. Firing the compacts in the CO_2 flow at 800 and 900 °C for 2 h resulted in an additional carbonatation on the B-sites and a further decrease in the sintering temperature to 890 °C. The compacts fired in the 900–1000 °C range became almost complete ceramics with high densities and mechanical properties close to those of medical implants. Firing at temperatures above 1000 °C resulted in an additional carbonatation on the A-sites. However, this led to a material with low densities and poor mechanical properties. A supposition has been proposed that the effect of CO_2 gas-activated sintering is a result of the intensification of the diffusion in the nanoparticles caused by CO_2 molecules entering the bulk from the CO_2 atmosphere and (or) releasing from the bulk due to the decomposition of carbonates on the B-sites in the lattice.

Keywords: Carbonated hydroxyapatite; Firing

1. Introduction

The carbonate ion, CO_3^{2-}, is an important substitution in hydroxyapatite (HA), $Ca_{10}(PO_4)_6(OH)_2$, of biological origin and it is processed by wet precipitation. CO_3^{2-} can substitute for OH^-, PO_4^{3-} or both resulting in A-type, AB-type or B-type carbonated hydroxyapatite (CHA), respectively.[1,2]

CHA ceramics have been studied comprehensively as prospective materials for orthopaedic, fluorescence and sensor applications.[3–5] However, some problems arose in processing CHA ceramics with the desired degree and mode (A-, AB- or B-types) of carbonatation. The CO_3^{2-} content in a ceramic was found to depend strongly on processing variables, mainly, on the CO_3^{2-} content and structural state of the initial powder used for compacting, but also on temperature, heating rate, duration and atmosphere of sintering, and the mode of substitution changes unpredictably during the heat-treatment.[6–15] In general it can be said that, the higher the CO_3^{2-} content in an initial powder is, the lower is its crystallinity and sintering temperature and, as a result, the higher is the carbonatation in the processed ceramics.[9,10,12,13] The use of CO_2 atmospheres (wet or dry) led to alterations in shrinkage rate and sintering temperature of the compacts and to changes in chemical and phase compositions and structural characteristics, like the type of carbonatation, of CHA ceramics.[3–5,8,11]

The overall situation gets even more complicated if the initial powder includes other impurities besides CO_3^{2-}. These stem usually from parent reagents, the synthesis reaction or powder-processing (like ions, intermediate phases or by-products, respectively). The impurities decompose and/or react in the lattice during heat-treating compacts of the powder.[16] These solid-state reactions highly affect the densification.[17]

After all, the sintering process of a CHA ceramic under the conditions described above has not yet been elucidated sufficiently. The aim of this study was to clarify the principal factors for lowering the sintering temperature and to reveal the role of CO_2 atmospheres for processing CHA ceramics with desired characteristics.

* Corresponding author. Tel.: +38 057 707 56 84.
E-mail addresses: intercom@univer.kharkov.ua, mykola.v.tkachenko@univer.kharkov.ua (Z. Zyman).

0955-2219/$ – see front matter © 2010 Elsevier Ltd. All rights reserved.
doi:10.1016/j.jeurceramsoc.2010.09.005

2. Materials and methods

In order to exclude the effect of other ions except CO_3^{2-} on sintering CHA's, the following procedure was used.[18] Precipitates were produced by a wet method employing the reaction of calcium carbonate and orthophosphoric acid.[19] Because of the negligible solubility of $CaCO_3$ in water,[20] the reaction was promoted by using a fine-grained $CaCO_3$ powder and the synthesis was carried out at 45 °C, which is an elevated temperature for a wet method. After grinding, a specific amount of $CaCO_3$ powder (Merck, Darmstadt, Germany, analytical grade) was dispersed in distilled water. A solution of H_3PO_4 (Merck) was rapidly poured into the $CaCO_3$ suspension under continuous mixing of the reaction medium.

The formed precipitate was centrifugalized, dried in an oven at 90 °C, ground in an agate mortar and sieved through a 100 μm sieve resulting in the initial powder. Compacts were made as pellets of 3 mm height and 10 mm diameter by pressing portions of the powder in a steel die under 120 MPa. The average porosity of the compacts was 51 ± 0.5%. The compacts were fired in a dry CO_2 flow (4 mL/min) in the range of 800–1200 °C with a 100 °C step and 2 h dwell-time at each temperature. Five batches of fired compacts were prepared with 10 samples each.

Structural analysis was performed using a Philips APDW 40C diffractometer and a copper K_α radiation ($\lambda = 0.154$ nm) with a nickel filter through 20–70° diffraction angles (2θ). IR spectra were recorded employing a BIO-RAD FFS 175 spectrometer (Germany) at a 2 cm^{-1} resolution and the KBr technique, operating in the transmittance mode between wave numbers of 400–4000 cm^{-1}. The morphology and microstructure of the samples were studied using an ESEM Qunta 400 scanning electron microscope (Germany).

Calcium amounts in the samples were determined by atomic absorption spectroscopy (Thermo Electron Corporation, M-series AA spectrometer). Corresponding amounts of orthophosphate were found by colorimetry using the molybdenum blue method (Varian Cary Win UV spectrophotometer, $\lambda = 725$ nm).

A thermogravimetric (TG) study of the samples was conducted up to 1200 °C in a N_2 flow of 50 mL/min (NETZSCH STA 409 PC/PG, Germany), air or a dry CO_2 flow of about 4 mL/min (MVT Instrument, Ukraine) at a heating rate of 5 K/min with the absolute error of the measurement being 2%. The dynamic shrinkage in the compacts was measured by dilatometry (MVT Instrument, Ukraine) using the same heating rate and atmospheric conditions as in the thermogravimetric study.

The density of the samples was measured by the Archimedes' principle using distilled water and average values for 10 samples in each batch. The relative density and the apparent porosity were calculated using 3.156 g/cm^3 as the theoretical density of stoichiometric HA. The error of the determination was less than 1%. The Vickers hardness of the fired compacts was determined using a PMT-3 microhardness tester (USSR) by applying an ultimate load of 2 N for 10 s. The compressive strength was measured employing an Instron-type testing machine.

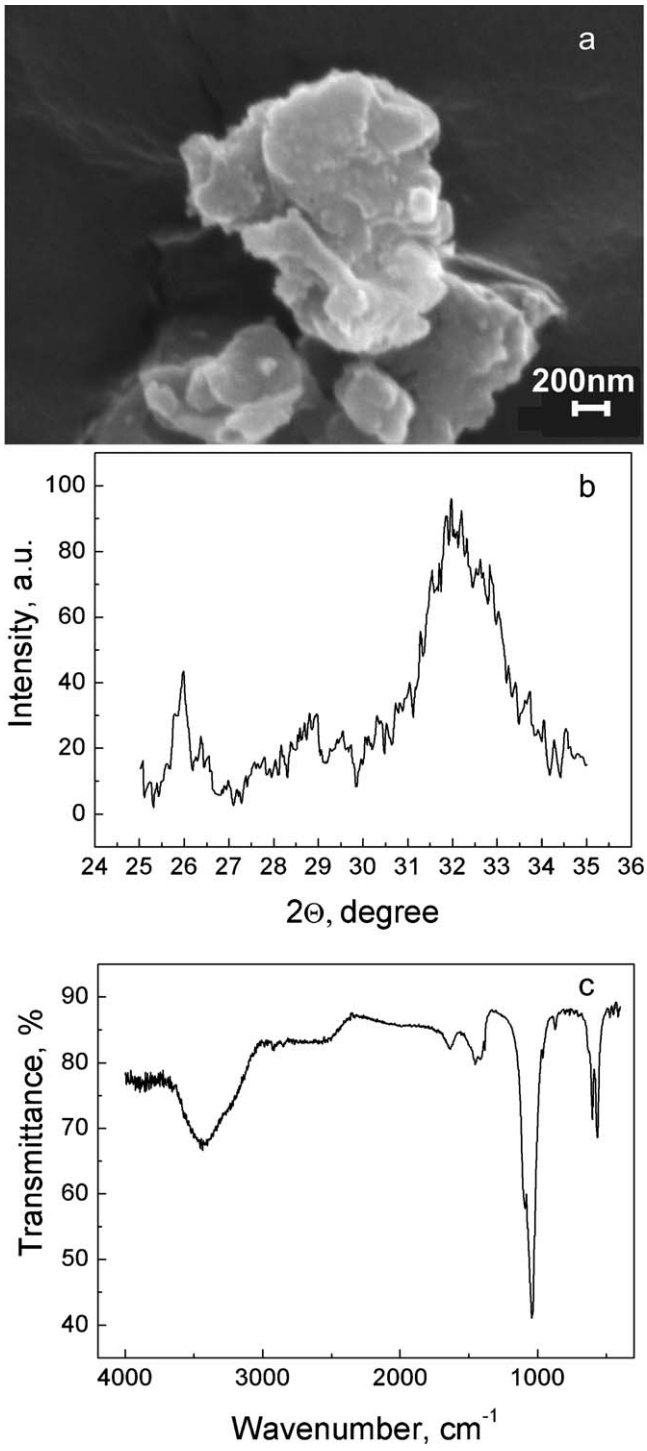

Fig. 1. Typical a – SEM micrograph, b – XRD pattern, and c – IR spectrum of the initial powder.

3. Results

3.1. Characterization of the initial powder

According to SEM pictures, the initial powder consists of particles with sizes in the wide range of 0.1–100 μm. However, each particle is consisted from tiny platelets of around 10^2 nm (Fig. 1a). XRD patterns of the powder manifest

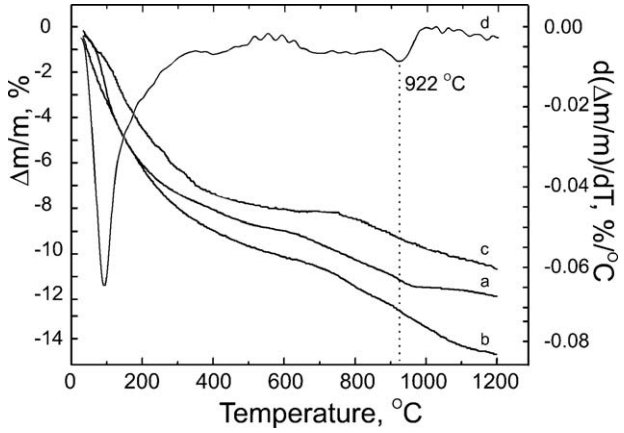

Fig. 2. TG curves of the initial powder in a – N_2 flow, b – air, and c – CO_2 flow; d – the DTG curve for the powder in the N_2 flow.

considerably broadened diffraction maxima positioned at diffraction angles 2θ as those of a nanocrystalline HA (Fig. 1b). IR spectra (Fig. 1c) show the absorption of PO_4^{3-} ions at 566, 602, 962, 1042, 1090 cm^{-1} and of lattice and adsorbed water at 1636 and 3440 cm^{-1}, respectively. Very weak shoulders at 3570 and 630 cm^{-1} indicate little amounts of OH^- groups in the lattice, additionally absorptions at 1416 and 1452 cm^{-1} of υ_3 CO_3^{2-} groups and 875 cm^{-1} of υ_2 CO_3^{2-} are present. Traces of CO_3^{2-} groups can be expected in a HA powder prepared by wet synthesis if no precaution for their elimination is taken.[6,17] Moreover, it is plausible to expect the presence of CO_3^{2-} ions in the HA as residual precipitates stemming from the applied reaction since the ions are a constituent of the $CaCO_3$ reagent. A sharp but weak band at 1385 cm^{-1} is associated with the NO_3^- impurities of the KBr used for sample preparation in the IR study.

A TG curve in case of heating the powder in a N_2 flow has two plateau-like sections. The temperature ranges of the sections are determined from the corresponding DTG curve at about 520–600 °C and 980–1060 °C (Fig. 2a and d). Therefore, the TG curve is divided into three parts of room temperature (RT) to 600 °C, 600–1000 °C, and 1000–1200 °C. Considering the nature of the gases released from a powder processed by the "nitrous" method during heating[21] and the fact that only H_2O and CO_3^{2-} might have been the impurities in the powder prepared in this study, it can be concluded that adsorbed and lattice water liberated in the RT to 600 °C range, CO_2 in the 600–1000 °C range, and water due to the dehydroxylation in the N_2 flow at temperatures above 1000 °C. As a result, mass losses of 8.8 wt% for H_2O (to 600 °C), 2.5 wt% for CO_2 (from 600 to 1000 °C), and 0.4 wt% for H_2O (above 1000 °C) are calculated from the curve, giving a total mass loss of 11.7 wt%. The CO_2 mass loss of 2.5 wt% is caused by the thermal decomposition of 3.4 wt% CO_3^{2-} in the lattice. This result is in acceptable agreement with an IR evaluation. Applying a calibration curve for a B-type CHA (CO_3^{2-} content vs $R_B = A_{1420}/A_{603}$, where A_{1420} and A_{603} were υ_3 CO_3^{2-} and υ_4 PO_4^{3-} absorbencies, respectively),[22] a value of 3.2 wt% for CO_3^{2-} in B position is found (for $R_B = 0.47$ from the IR spectrum of the initial powder, Fig. 1c). In accordance

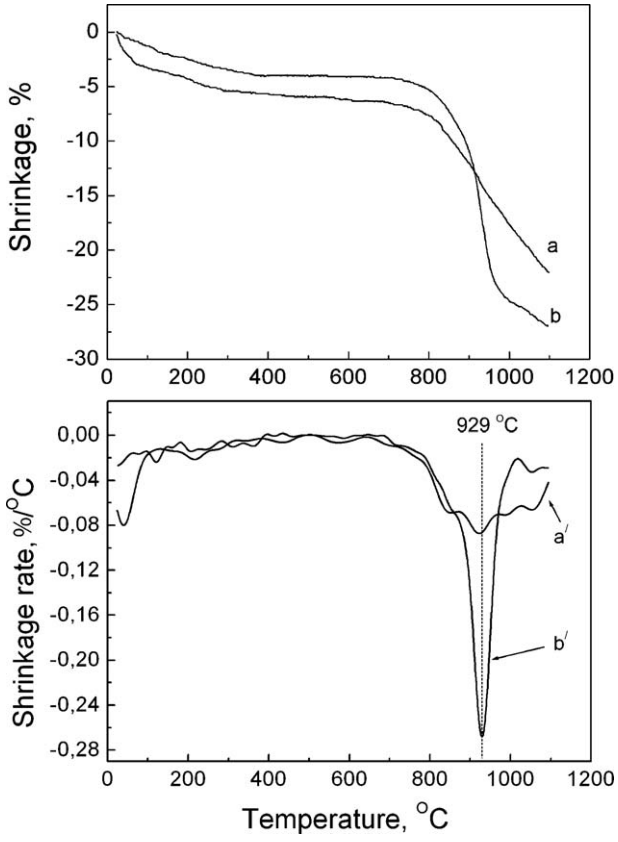

Fig. 3. Curves of the shrinkage and shrinkage rate for the compacts during heating in a, a′ – air, and b, b′ – the CO_2 flow.

with the characteristics of IR bands and 3.4 wt% CO_3^{2-} content (Figs. 1c and 2a), the initial powder is a slightly carbonated B-type HA.[23,24]

The amount of CO_2 released from the powder in air (2.6 wt%) is the same like in N_2 (2.5 wt%) under equal conditions (Fig. 2b; the experimental error is ±0.1 wt%). N_2 atmosphere (flow) and air have a negligible effect on the mass loss in the 600–1000 °C range. However, the CO_2 flow has. The total mass loss in the powder heated to 1200 °C in the CO_2 flow is 10.6 wt% (Fig. 2c), including 8.2 wt% mass loss from RT to 600 °C, 1.6 wt% from 600 to 1000 °C and 0.8 wt% for temperatures above 1000 °C, compared to the total 14.2 wt% mass loss in air, including 10.2 wt%, 2.7 wt% and 1.3 wt%. The amount of released CO_2 is almost two times less than that in air. It is assumed that the reduction in mass loss is caused by the formation of new CO_3^{2-} groups formed by CO_2 molecules taken up from the flow. These new carbonates partly compensate those decomposed and released as CO_2 during heating. In that case, there still are 3.4 wt%–2.2 wt% = 1.2 wt% CO_3^{2-} in the initial CHA powder heated to 1000 °C in the CO_2 flow.

3.2. Shrinkage of the powder compacts

Shrinkage of the powder compacts, containing 3.4 wt% CO_3^{2-} initially, starts at about 700 °C while heating in air (Fig. 3a). The shrinkage rate increases with increasing temperature and reaches a maximum at about 930 °C and decreases

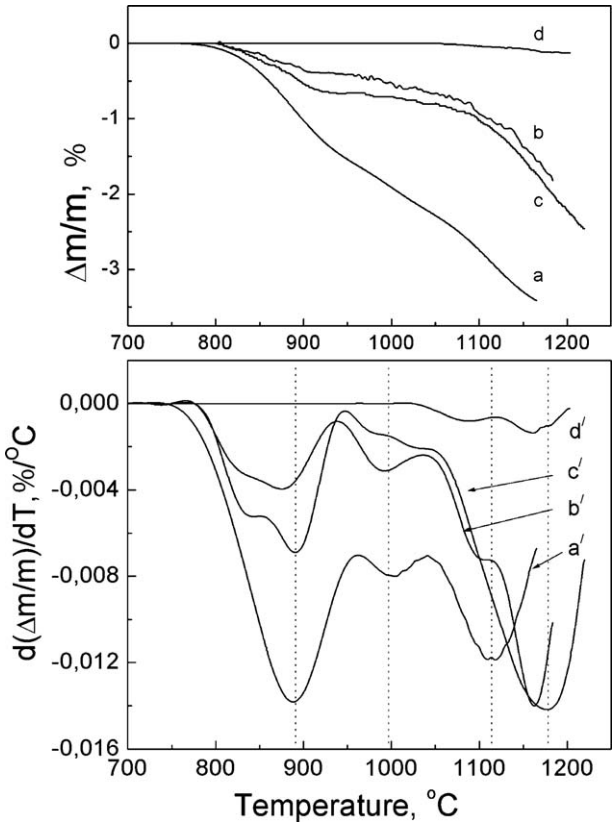

Fig. 4. TG and DTG curves of the compacts in air preliminary fired in the CO_2 flow for 2 h at a, a′ – 800, b, b′ – 900, c, c′ – 1000 °C, and d, d′ – 1100 °C.

afterwards at higher temperatures (Fig. 3a′). An impressive effect is observed in case of heating similar compacts in the CO_2 flow. The shrinkage commences and the shrinkage rate passes through a maximum at about the same temperatures as in air (Fig. 3b and b′). However, the maximum rate of shrinkage in CO_2 is more than three times higher than that in air. The beginning and the development of the shrinkage displayed on the temperature scale are consistent with the process of mass loss due to CO_2 liberation in N_2. Moreover, the temperatures of the maximum rates of the gas release and the shrinkage almost coincide (922 and 929 °C, Figs. 2d and 3a′, b′).

CO_2 gas liberation from incompacted CHA powder may differ from that of compacted powder.[11] Also, shrinkage may not result in sintering.[12,13] Besides, the CHA powder displays less mass loss while heating in CO_2 as that in N_2 or air (Fig. 2). Considering this and the desire to strengthen the observed gas-activated effect and to develop an approximate heat-treatment for sintering, the compacts are fired in a CO_2 flow for 2 h at temperatures of 800, 900, 1000, 1100 and 1200 °C.

For compacts fired at 800 °C, the mass loss in the 800–1000 °C range in air is 1.9 wt% (Fig. 4a), i.e. higher than the 1.2 wt% of the initial powder (Fig. 2b). Consequently, some carbonatation happens in the compacts during firing. The corresponding DTG curve (Fig. 4a′) displays a maximum in the rate of mass loss at 890 °C. This temperature is somewhat lower than that of the maximum rate of shrinkage in the dilatometric test (Fig. 3b′). Temperatures of the maximum rate of

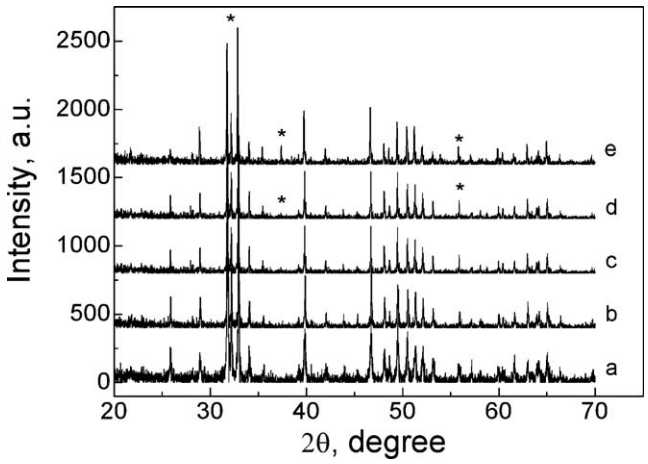

Fig. 5. XRD patterns of the compacts upon firing in the CO_2 flow for 2 h at a – 800, b – 900, c – 1000, d – 1100 °C, and e – 1200 °C.

shrinkage (sintering temperatures) in CHA powder compacts are found to decrease as the carbonate content in the initial powder increases.[9,10] Hence, the two temperatures of the maximum rates of shrinkage and mass loss (929 and 890 °C) can be considered as an indicator for the same process because the carbonate content in the compact fired at 800 °C is slightly higher than that in the initial powder. The other results in Fig. 4 are discussed further.

A minor acceleration is found in the shrinkage during heating the compacts in air (Fig. 3a′). The initial carbonate ions are decomposed almost completely, and the CO_2 molecules formed of the fractions are released from the lattice to 1000 °C. The N_2 and air atmospheres had negligible effect on this process (Figs. 2a, b and 3a′). However, while heating a compact in the CO_2 flow, a CO_2 uptake into the lattice takes place. There exist two opposite CO_2 streams, one into the bulk of particles, which resulted in the new CO_3^{2-} formation, and another stemming from the particles because of the thermal CO_3^{2-} decomposition in the lattice (as in air or N_2). This partial exchange with CO_2 between the crystallites and the gaseous medium might have caused alterations in the amount and position of carbonates and, consequently, in the lattice characteristics.

3.3. Densification of the compacts fired in a CO_2 flow

XRD patterns show no changes in the phase composition for the compacts fired at 800, 900 and 1000 °C (Fig. 5a–c): exclusively characteristic CHA peaks appear. Only few CaO was formed in the samples fired at 1100 °C, and the CaO content slightly increases in the compacts fired at 1200 °C. This can be followed from the presence of very weak characteristic CaO reflections and a slight increase of their intensities in the corresponding patterns (Fig. 5d and e) besides the CHA peaks.

The increased sharpness of the diffraction profiles, compared to those in Figs. 1b and 5, enables the determination of the lattice constants for the fired compacts. The obtained values (Fig. 6) for the lattice constant *a*, the constant *c* showed slighter changes, of the material after firing the compacts at 800 and 900 °C are markedly lower than the 9.418 Å of stoichiometric HA.[25] Such a decrease is usually attributed to the CO_3^{2-} substitution for

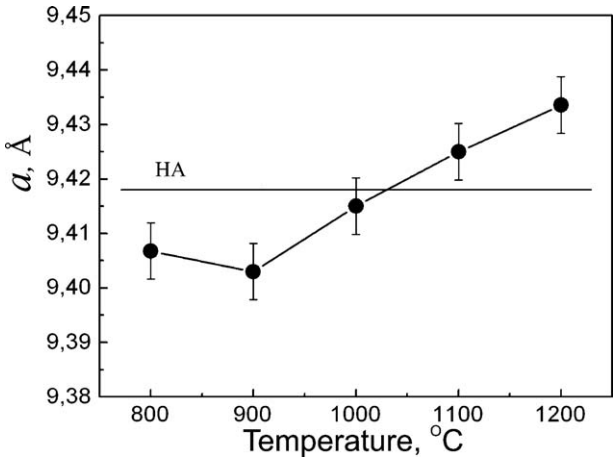

Fig. 6. The lattice constant a vs firing temperature of the CHA compacts.

PO_4^{3-} ions.[26] The concentration of CO_3^{2-} on B-sites causes the observed decrease of a to 9.407 Å (800 °C) and 9.403 Å (900 °C) considering that CO_3^{2-} ions in the phosphate positions tend to reduce the a-parameter by 0.006 Å/wt% CO_3^{2-}.[24,26,27] The calculations show that (9.418–9.407 Å)/0.006 Å/wt% = 1.83 wt% and (9.418–9.403)/0.006 Å/wt% = 2.5 wt% of CO_3^{2-} occupy the B-sites after firing the compacts at 800 °C and 900 °C, respectively. Because the carbonate content in the initial powder after heating in the CO_2 flow to 900 °C is (according to c-curve in Fig. 2) 3.4–1.6 wt% = 1.8 wt% (the CO_2 mass loss was 1.15 wt%), it can be concluded that B-site carbonatation occurs during firing the compacts at 900 °C. The picture radically changes for the compacts fired above 900 °C. The a-constant increases, and the values plotted versus temperature result in a nearly linear dependence (Fig. 6). This is typical for an A-type substitution in CHA when the CO_3^{2-} groups occupy the OH^- positions.[26]

IR spectra of the fired compacts (Fig. 7) confirm the XRD data and give additional information. In principal, an IR spectrum of the compact fired at 800 °C has the same characteristics as that of the initial powder (Figs. 7a and 1c). However, some

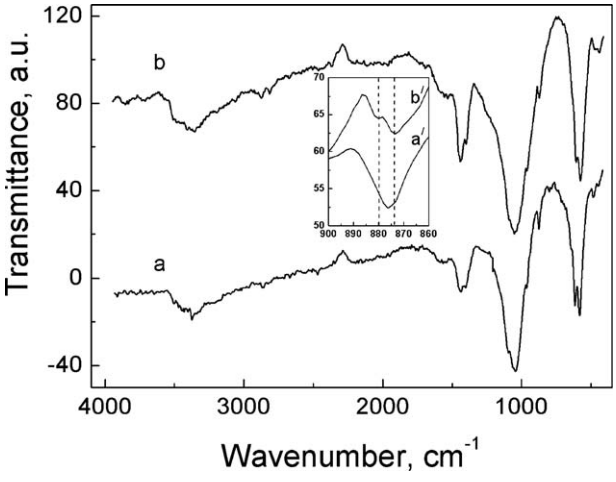

Fig. 7. IR spectra of the compacts fired in the CO_2 flow for 2 h at a, a′ – 800 °C, and b, b′ – 1000 °C. The insert – an extended υ_2 CO_3^{2-} range.

Table 1
Density (ρ), Vickers microhardness (H_υ) and compressive strength (σ_c) of the compacts fired at various temperatures (T_f) for 2 h in the CO_2 flow.

T_f (°C)	ρ (g/cm^3)	H_υ (±10%) (MPa)	σ_c (±10%) (MPa)
800	2.65 ± 0.01	127	219
900	2.88 ± 0.01	156	224
1000	2.97 ± 0.01	171	200
1100	2.23 ± 0.01	118	14
1200	2.26 ± 0.01	126	25

distinguishing features appear in spectra of the compacts fired at temperatures above 800 °C. For the compacts fired at 1000 °C (Fig. 7b), clear peaks and more or less resolved shoulders at 1410, 1450, 1460, 1475, 1500, 1515 cm^{-1} and, particularly, at 1545 and 1570 cm^{-1} in the υ_3 CO_3^{2-} region are present indicating an AB-type CHA.[6,28] Instead of a sharp absorption at 875 cm^{-1}, a doublet appears, though poorly resolved but clearly discerned, at 873 and 880 cm^{-1} in the υ_2 CO_3^{2-} region (the inset in Fig. 7). The ratio of the intensities of the peaks at 880 and 873 cm^{-1}, corresponding to the ratio of A-type/B-type substitution,[6] is 0.49, indicating that there are insignificantly more carbonate groups on the B-site than on the A-site in the lattice. However, the ratio of the intensities increased to 0.95 for the ceramics fired at 1200 °C denoting that the relative amount of CO_3^{2-} on the A-sites increases, which is in full agreement with an increase of a in the 900–1200 °C firing range (Fig. 6). Another important feature is the broadening of the PO_4^{3-} bands as the firing temperature of the compacts is increased (Fig. 7a and b) which results in a gradual loss of resolution in the spectra. Such broadening is usually associated with a decrease in crystallinity of HA.[29] Most likely the broadening in the spectra of the compacts fired at and above 1000 °C is associated with the decrease in crystallinity because of the development of stresses in the lattice as the carbonate is known to cause distortions in the HA structure. Since the carbonate ions on A-positions distort the lattice more than on B-positions,[22] the crystallinity in the fired compacts decreases as the relative amount of the A-type substitution increases with an increase in firing temperature.

The microstructure, density and mechanical properties (microhardness and compressive strength) were studied to clarify how the shrinkage is associated with sintering in the fired compacts. The microstructure of a fractured compact after firing at 800 °C reveals powder particles fused together to a certain degree (Fig. 8a). The relative density of the compact is 84%, i.e. around 16% of the initial porosity in the compact (51%) are still present (Fig. 9 and the Table 1). The porosity decreases and both density and microhardness increase to maximum values as the firing temperature is increased to 1000 °C. The compacts transform into ceramics after firing at 1000 °C with their fractured surface showing grains of micron sizes with developed internal microstrains because of the distortions (Figs. 8b, c and 9; Table 1). Firing at temperatures above 1000 °C results in a drastic decrease in density and mechanical properties. This is associated with the occurrence and growth of tiny particles on the surfaces of grains (Fig. 8d). Elemental analysis of the powder samples gave a calcium content of 39.4 wt % and a phosphate content

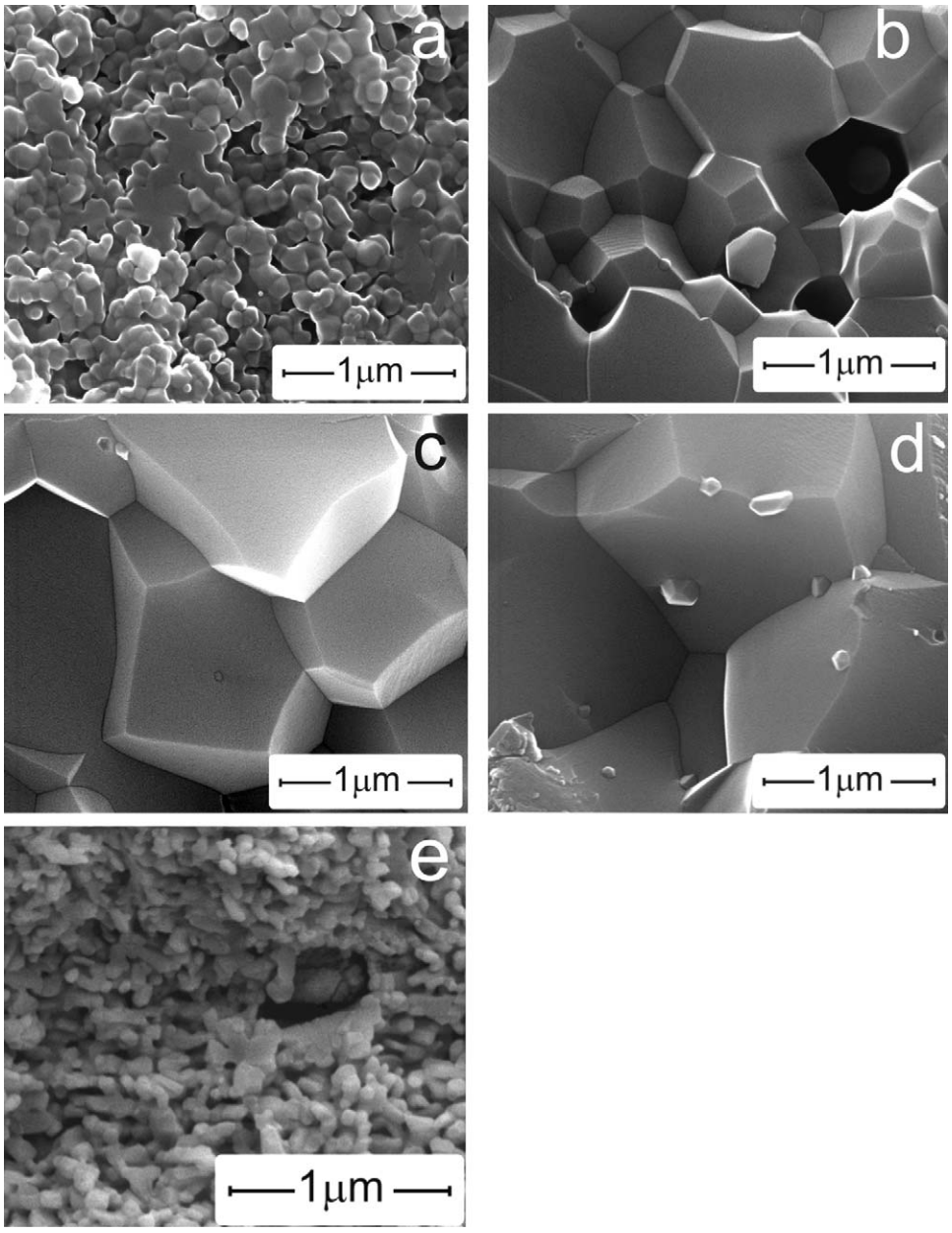

Fig. 8. The surface microstructure of the fractured compacts fired for 2 h in the CO_2 flow at a – 800, b – 900, c – 1000, d – 1100 °C, and in air at e – 1000 °C.

of 52.4 wt % which corresponds to a Ca/P ratio of 1.79. Firing powder compacts with a ratio higher than the stoichiometric value of HA (1.67) at and above 1000 °C is known to result in the formation of CaO in the ceramics.[30] This is well consistent with the CaO reflections detected in the XRD patterns of the corresponding samples (Figs. 5d and e). The CaO particles most likely cause a loosening of the grain boundaries and weaken the ceramic.

The rapid shrinkage at 929 °C results in sintering and the formation of ceramics. Unfortunately, the effect of firing temperature on the characteristics of the sintered compacts is not detailed from 900 to 1000 °C. However, considering the assumed view of the density curve in this range (the dashed lines in Fig. 9), one might expect that the maximum density and the highest mechanical characteristics are actually achieved at a firing temperature between 900 and 1000 °C (around 985 °C), i.e. in the range of maximum activation of the shrinkage due to CO_2 liberation. Contrary to this, the porosity is still open in the compacts fired at 1000 °C in air as can be seen in the micrographs (Fig. 8e). Since the sintering temperature of an AB-type CHA (the assumed value is 985 °C) is higher than that of a mainly B-type CHA (929 °C), it can be supposed that a CHA sintering temperature depends not only on the content but also on the mode of CO_3^{2-} distribution in the two lattice positions with a tendency to increase as the A/B ratio increases.

The obtained results contribute to a further clarification of the dependences in Fig. 4. As it is mentioned above, the porosity in the compacts after firing at 800 °C in the CO_2-flow is 16%, i.e. roughly one third of the initial porosity in the compacts (51%) is still present. Due to the remaining open porosity, about

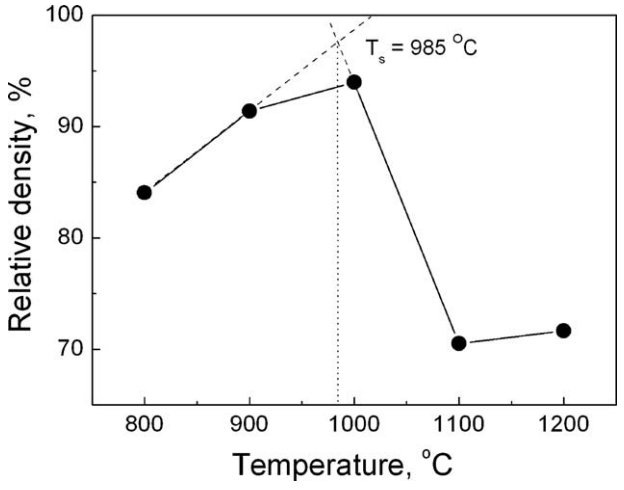

Fig. 9. The relative density vs temperature in the compacts fired for 2 h in the CO_2 flow.

3.45 wt% of CO_2 are released up to 1170 °C during a TG run (in air) from the compact (Fig. 4a). This mass loss results from the decomposition of 4.7 wt% of CO_3^{2-} in the lattice. The amount of the mass loss is an additional proof for the carbonatation during firing the compact (the initial carbonate content in the powder is 3.4 wt%). Firing at 900 and 1000 °C yielded sintered ceramics because the residual porosities in the compacts are 9% and 6%, respectively (Fig. 9). As a consequence, the mass loss in both of them to 1170 °C is about 1.6 wt% of CO_2 (Fig. 4b and c), i.e. more than twice as less than for the compact fired at 800 °C. The gas release from the compacts (ceramics) after firing at temperatures above 1000 °C decreases dramatically which is most likely attributed to the loss of the initial carbonate while heating to these high temperatures (Fig. 4d and d′).

Three main maxima in gas release are observed at 890, about 1000, and in the 1110–1180 °C range for the compacts fired at 800, 900 and 1000 °C in the CO_2 flow. The first maximum is attributed to the decomposition of CO_3^{2-} ions on the B-sites. The weak second one is mainly caused by the decomposition of carbonates on the A-sites and CO_2 liberation from the almost fully dense grains. The third maximum in the high temperature range is supposed to appear because of the decomposition of the residual carbonates and, most likely, because of the loss of some OH^- groups. The density of the sintered ceramics decreases drastically after firing at temperatures above 1000 °C (Table 1 and Fig. 9), and this enables the liberation of the indicated pieces. The rate of mass loss at around 1170 °C is the same as that at 890 °C of the compact with open porosity which is an additional argument for the presented picture.

4. Discussion

Based on the above results, a new supposition on the nature of the CO_2-activated sintering is proposed. Substantial activation in sintering happens at about 900 °C during firing the compacts in the CO_2 atmosphere (Fig. 3). Simultaneously, the firing results in a carbonatation of HA (mainly in B-sites; Fig. 6). Heating the compacts with different amounts of CO_3^{2-} in the N_2-atmosphere or air with no or a negligible amount of CO_2 reveals a considerable rate of mass loss due to the decarbonatation in the lattice at about 900 °C (Figs. 2d and 4a′–c′). Hence, there are two opposite CO_2 streams while firing the compacts: the one goes from the CO_2 atmosphere into the bulk of the apatite particles, and the other one the way round. Uptake and (or) release of CO_2 molecules from the particles may activate the ion diffusion (likely, both the volume and the surface migrations) which results in sintering at much lower temperatures (around 900 °C) than usual for conventional HA sintering (1150–1200 °C[1,2,19]). However, the activation only proceeds at firing temperatures up to about 1000 °C. At higher temperatures, the carbonatation takes part on the A-sites (Figs. 6 and 7). This leads to a filling of the hexed channels and blocks (restricts) with a release of decomposed CO_3^{2-} molecules from the lattice. As a result, the activation process is weakened drastically.

Proceeding on this supposition on the nature of the CO_2 gas-activated sintering, a different view on some earlier findings in sintering CHA's can be proposed. For instance, a decrease in sintering temperature with an increase of carbonate content in an initial CHA powder was associated with simultaneous dispersion of the powder.[10] The dispersion may actually stimulate sintering due to the increased role of the surface diffusion. However, significantly different sintering temperatures were found for the same carbonatation (and, consequently, similar dispersity) in CHA compacts in another study.[9] Based on our supposition, the discrepancy can be explained by the use of different sintering atmospheres in the studies, namely CO_2 vaporized with water[9] and a flow of dry Ar.[10] The strong effect of the kind of gas atmosphere on the CO_3^{2-} loss in a CHA and, consequently, on the CO_2 stream intensity at a definite (sintering) temperature is clearly seen in Fig. 3. According to another finding,[11] the decrease in sintering temperature is attributed to an increasing amount of sodium substituted for calcium with an increase in carbonate content. Sodium is supposed to form an easily melting compound promoting the shrinkage. However, a decrease of about 230 °C in the sintering temperature in dry CO_2 compared to that in air was observed in this study (Fig. 3), when no sodium containing parent reagents were used for the synthesis. Finally, peculiarities in the shrinkage curve in the 700–1000 °C firing range in air are observed for compacts having similar dispersities but differing in the CO_3^{2-} contents.[17] The peculiarities are strongly associated with the gas release (mass loss) of the compacts. Compacts of pure HA usually have a smooth shrinkage curve.

5. Conclusions

Densification of compacts of slightly carbonated hydroxyapatite nanoparticles under conditions of heating from RT to 1200 °C is highly effected by a CO_2 gas flow in the 600–1000 °C range. Air and flowing N_2 had slight and negligible effects on the densification. However, the flow of dry CO_2 promotes an increase in the shrinkage rate of the compacts at 929 °C thrice as high. A mass loss in the compacts accompanies the densification. The mass loss is caused by the release of CO_2 owing to the decomposition of carbonates on the B-sites in the CHA lattice.

Firing the compacts in the CO_2 flow at 800, 900 and 1000 °C for 2 h yields an increase in the carbonate content in the fired compacts and almost dense ceramics (after firing at 1000 °C). Depending on the treatment conditions, the sintering temperature of the compacts decreases by 260 °C: from about 1150 °C in air of HA to 890 °C in the CO_2 flow of CHA. The CHA ceramics have mechanical characteristics suitable for a use as medical implants. Similar firing of the compacts at temperatures above 1000 °C results in ceramics with an increase of carbonatation on the A-sites. However, these ceramics show a drastic decrease in density and mechanical properties.

A new supposition on the nature of the CO_2 gas-activated sintering that partially results in the decrease of the sintering temperature has been proposed. According to the supposition, the CO_2 streams from the CO_2 atmosphere into the bulk and (or) vice versa, owing to the CO_3^{2-} decomposition in the lattice, activate the diffusion processes in the CHA nanoparticles and promote sintering.

Acknowledgments

This work was supported by the Fundamental Researches State Fund of the Ministry of Education and Science of the Ukraine under contract F28/248-2009. The authors are grateful to Prof. M. Epple (Duisburg-Essen University, Germany) for providing some modern equipment for checking measurements.

References

1. Epple M, Baeuerlein E, editors. *Biomineralisation. Medical and clinical aspects*. Weinheim: Wiley-VCH; 2007.
2. Ratner BD. *Biomaterials science: an introduction to materials in medicine*. Elsevier Academic Press; 2004.
3. Landi E, Tampiery A, Celotti G, Vichi L, Sandri M. Influence of synthesis and sintering parameters on the characteristics of carbonate apatite. *Biomaterials* 2004;**25**:1763–70.
4. Lafon JP, Champion E, Bernache-Assollant D, Gibert R, Danna AM. Thermal decomposition of carbonated calcium phosphate apatites. *J Therm Anal Calorim* 2003;**72**:1127–34.
5. Barralet JE, Fleming GJP, Campion C, Harris JJ, Wright AJ. Formation of translucent hydroxyapatite ceramics by sintering in carbon dioxide atmospheres. *J Mater Sci* 2003;**38**:3979–93.
6. Gibson IR, Bonfield W. Novel synthesis and characterization of an AB-type carbonate-substituted hydroxyapatite. *J Biomed Mater Res* 2002;**59**:697–708.
7. Yasukawa A, Kandori K, Ishikawa T. TPD–TG–MS study of carbonate calcium hydroxyapatite particles. *Calcif Tissue Int* 2003;**72**:243–50.
8. Barralet J, Knowles JC, Best S, Bonfield W. Thermal decomposition of synthesized carbonate hydroxyapatite. *J Mater Sci: Mater Med* 2002;**13**:529–33.
9. Ellies LG, Nelson DGA, Featherstone JDB. Crystallographic structure and surface morphology of sintered carbonated apatites. *J Biomed Mater Res* 1988;**22**:541–53.
10. Doi Y, Koda T, Wakamatsu N, Goto T, Kamemizu H, Moriwaki Y, et al. Influence of carbonate on sintering of apatites. *J Dent Res* 1993;**72**(9):1279–84.
11. Doi Y, Koda T, Adachi M, Wakamatsu N, Goto T, Kamemizu H, et al. Pyrolysis-gas chromatography of carbonate apatites used for sintering. *J Biomed Mater Res* 1995;**29**:1451–7.
12. Merry JC, Gibson IR, Best SM, Bonfield W. Synthesis and characterization of carbonate hydroxyapatite. *J Mater Sci: Mater Med* 1998;**9**:779–83.
13. Barralet JE, Best SM, Bonfield W. Effect of sintering parameters on the density and microstructure of carbonate hydroxyapatite. *J Mater Sci: Mater Med* 2000;**11**:719–24.
14. Rodriguez-Lorenzo LM, Vallet-Regi M. Controlled crystallization on calcium phosphate apatites. *Chem Mater* 2000;**12**:2460–5.
15. Tonsuaadu K, Peld M, Leskela T, Mannonen R, Niinisto L, Veiderma M. A thermoanalytical study of synthetic carbonate-containing apatites. *Thermochim Acta* 1995;**256**:55–65.
16. Zyman Z, Rokhmistrov D, Ivanov I, Epple M. The influence of foreign ions on the crystal lattice of hydroxyapatite upon heating. *Mat-Wiss u Werkstofftech* 2006;**37**(6):530–2.
17. Zyman Z, Ivanov I, Rokhmistrov D, Glushko V, Tkachenko N, Kijko S. Sintering peculiarities for hydroxyapatite with different degree of crystallinity. *J Biomed Mater Res* 2001;**54**:256–63.
18. Zyman ZZ, Tkachenko MV, Polevodin DV. Preparation and characterization of biphasic calcium phosphate ceramics of desired composition. *J Mater Sci: Mater Med* 2008;**19**:2819–25.
19. Narasaraju TSB, Phebe DE. Some physico-chemical aspects of hydroxyapatite. *J Mater Sci* 1996;**31**:1–21.
20. Knunyanc IL.*The chemical encyclopedic vocabulary*. Moscow: Sovet Encyclopedia Press; 1983.
21. Zyman ZZ, Rokmistrov DV, Glushko VI, Ivanov IG. Thermal impurity reactions and structural changes in slightly carbonated hydroxyapatite. *J Mater Sci: Mater Med* 2009;**20**:1389–99, doi:10.1007/s10856-009.3706-4.
22. Clasen ABS, Ruyter IE. Quantitative determination of type A and B carbonate in human deciduoces and permanent enamel by means of Fourier transform infrared spectrometry. *Adv Dent Res* 1997;**11**(4):523–7.
23. Nelson DGA, Featherstone JDB. Preparation, analysis, and characterization of carbonated apatites. *Calcif Tissue Int* 1982;**34**:S69–81.
24. Vignoles M, Bonel G, Holcomb DW, Young RA. Influence of preparation conditions on the composition of type B carbonated hydroxyapatite and on the localization of the carbonate ions. *Calcif Tissue Int* 1988;**43**:33–40.
25. Koutsopoulos S. Synthesis and characterization of hydroxyapatite crystals: a review study on the analytical methods. *J Biomed Mater Res* 2002;**62**:600–12.
26. LeGeros RZ, Ttrauts OR, Klein E, LeGeros JP. Two types of carbonate substitution in the apatite structure. *Experientia* 1969;**25**(1):5–7.
27. Arias JL, Mayor MB, Garcia-Sanz FJ, Pou J, Leon B, Perez-Amor M, et al. Structural analysis of calcium phosphate coating produced by pulsed laser deposition at different water–vapor pressures. *J Mater Sci: Mater Med* 1997;**8**:873–6.
28. Rey C, Renugopalakrishnan V, Collins B, Glimcher MV. Fourier transform infrared spectroscopic study of the carbonate ions in bone mineral during aging. *Calcif Tissue Int* 1991;**49**:251–8.
29. Termine JD, Posner AS. Infrared analysis of rat bone: age dependency of amorphous and crystalline mineral fractions. *Science* 1966;**153**:1523–5.
30. Royer A, Vique JC, Heughebaert M, Heughebaert JC. Stoichiometry of hydroxyapatite: influence on the flexural strength. *J Mater Sci: Mater Med* 1993;**4**:76–82.